Demonstration of Inter-Chip RF Data Transmission Using On-Chip Antennas in Silicon Photonics

Bahaa Radi, *Student Member, IEEE*, Ajaypal Singh Dhillon, *Student Member, IEEE*, and Odile Liboiron-Ladouceur, *Senior Member, IEEE*

***Abstract*— This letter describes the design and the measurements of a 15 GHz monopole antenna implemented in silicon photonics for inter-chip communication. The antenna is designed in HFSS with its radiation pattern simulated. To confirm its operation and experimentally demonstrate inter-chip communication, the antenna is fabricated in a commercial Silicon Photonics fabrication process. Measurements include s-parameter using a vector network analyzer, and inter-chip data transmission between two on-chip antennas. The inter-chip data transmission is demonstrated using an off-chip photodetector directly as a transmitter as a proof-of-concept. Results indicate the feasibility of a monolithically integrated photodiode-antenna system as a transmitter.**

***Index Terms*— Antennas, wireless communication, passive circuits, silicon photonics, photodetectors.**

I. Introduction

RECENTLY, there has been an increasing interest in the implementation of front-end electronics with optical passives in silicon-photonics (SiP) [1]–[5]. There are several examples of such integration. A low-pass RC at the output of a photodetector in SiP can potentially be used as an envelope detector [1]. An RC matching network matches the output impedance of a photodetector to a 50 Ω load for optimum interface to a test and measurement equipment or an antenna [2]. Optimized on-chip peaking inductor extends the bandwidth extension and responsivity of photodetectors [3]. Finally, an optical passive delay line replaces the clock generation blocks of a conventional electronic receiver [4], [5]. This trend is possible partly due to the SiP platform proving to be a cost-effective option to host bulky electronic passives compared to high-end complementary metal-oxide-semiconductor (CMOS) platforms. More importantly for RF operation, the low conductivity of the substrate in the SiP stack allows for the implementation of electronic passives with high-quality factors. This low substrate conductivity is favorable for antennas preventing electromagnetic waves from being dissipated as heat in the substrate, thus improving the overall efficiency of the system [6]. Moreover, radio-over-fiber (RoF) applications are gaining commercial interest [7]. As such, researchers are developing critical components needed to support these applications [8]–[12] including mode-locked laser diode for RF frequency operation [8], high output power photodetectors [8]–[10], photomixers [8], [11], photonic transmitters [12], photonic-antenna emitters [13], [14], and integrated photoreceivers [15].

Following these new opportunities enabled by the emergence and advancement in photonic integration, we developed a planar monopole antenna for inter-chip RF communication and RoF applications leveraging a commercial SiP technology platform. The monopole antenna consists of one half of a dipole antenna with a ground plane acting as a mirror. SiP allows for monolithically integrating the antenna with the photodetector for a compact design with improved efficiency by the virtue of high substrate resistivity. Impedance matching between the photodetector and the antenna achieves optimal power transfer [16], [17]. The matching network can be removed with the photodetector close to the antenna further motivating the design of an antenna in silicon photonics.

In this letter, a 15 GHz monopole antenna is designed and measured. The antenna is fabricated in the commercially available silicon photonics process offered by Advanced Micro Foundry (AMF). Section II describes the structure of the designed antenna with the HFSS simulation results. Section III describes the S-parameter measurements validating the performance of the antenna. A pair of antennas on two different chips experimentally achieve inter-chip data communication. Finally, section IV concludes the work.

II. Antenna Design

The layout of the designed antenna is shown in Fig. 1(a). Here we choose a monopole antenna for its small size and the expected relatively uniform radiation pattern in the horizontal direction making it suitable for inter-chip communication. The fabrication layers of the AMF fabrication process are shown in Fig. 1(b) and consists of two metal layers.

A quarter-wavelength monopole antenna is a single-ended fed antenna one-half the size of a dipole antenna. The ground plane, which acts as a mirror, creates a field above the ground that is identical to one generated by a dipole antenna but with no field beneath it. The irradiated field can be calculated by image theory, which states that the fields above a perfectly conducting plane from a primary source are found by summing the contributions of the primary source and its image [18]. This means that a monopole structure orthogonal to the ground

Manuscript received January 24, 2020; revised March 23, 2020; accepted April 22, 2020. Date of publication April 29, 2020; date of current version May 12, 2020. This work was supported in part by the Canadian Microelectronic Corporation (CMC) for the subsidized MPW fabrication through A∗STAR Institute of Microelectronics and in part by the Natural Sciences and the Canada Research Chair programs. *(Corresponding author: Bahaa Radi.)*

The authors are with the Department of Electrical and Computer Engineering, McGill University, Montreal, QC H3A 0E9, Canada (e-mail: bahaa.radi@mail.mcgill.ca).

Color versions of one or more of the figures in this letter are available online at http://ieeexplore.ieee.org.

Digital Object Identifier 10.1109/LPT.2020.2991118

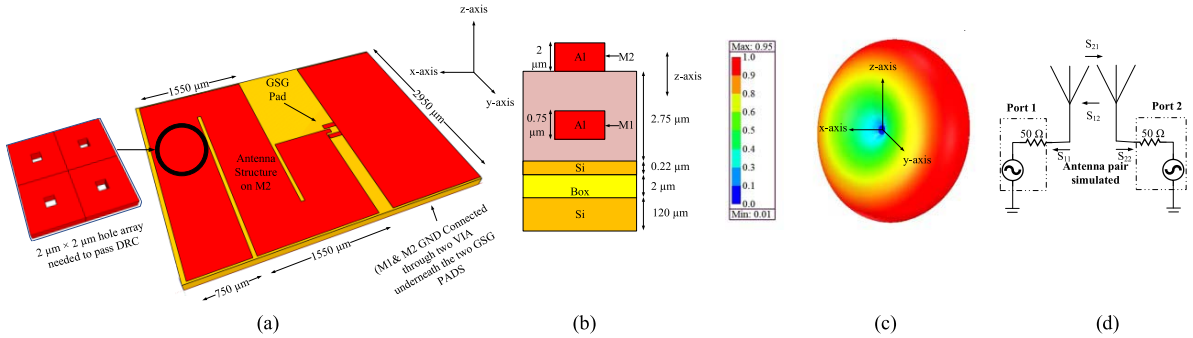

Fig. 1. (a) Layout of the fabricated antenna. (b) Stack layers of the AMF SiP fabrication process used to fabricate the antenna. (c) The simulated donut-shaped gain of the antenna in the far-field region. This gain is valid in the far region of operation. (d) The Model used for s-parameter simulations.

plane behaves as a dipole antenna, but with less radiation impedance since it is single-ended. The body of the antenna is implemented on the top metal (M2), while the ground plane is implemented on both metal layers M1 and M2 connected through a via. The SiP process features a relatively thin undoped silicon substrate (120 μm) below the insulator (Box in Fig. 1(b)). One advantage of the thin insulator is that post-processing, namely substrate etching, is not required to achieve good air radiation. Indeed, substrate etching is required when the process used features a thick substrate with high permittivity that leads to the electromagnetic waves radiating towards the silicon substrate instead of air [19]. Moreover, if the substrate is conductive, electromagnetic power is dissipated as heat degrading the radiation efficiency of the antenna [6]. This highlights the technological advantages of SiP technology as an antenna friendly, simple, and cost-effective process.

For a 15 GHz RF carrier in air, the length L of the planar monopole antenna in air is initially set to a quarter of the carrier wavelength $\left(L = \lambda_0/4\right)$.While the antenna length should be 5.800 mm in free space, simulations show that for the SiP process it needs to be is 8.125 mm at 15 GHz. In theory for optimal operation, the ground plane should extend to at least a quarter wavelength. However, the ground plane is shortened to 1.330 mm to reduce the size and cost of the fabricated antenna. Because the ground plane extends to less than the quarter wavelength necessary for proper operation, the length of the antenna is increased [20]. Simulations show that this smaller than ideal ground will reduce antenna gain by 0.368 (28%).

To reduce the overall size of the design, the antenna layout in an "S" shape. The antenna will have a more uniform horizontal radiation pattern at the cost of reduced gain in the direction of maximum directivity (yz plane). The simulated gain of the antenna is shown in Fig. 1(c). Antenna gain defines how directional the antenna is in a given direction compared to an isotropic antenna, but also takes radiation losses into account. The gain has the expected donut shape. The peak gain is 0.95 (-0.22 dBi), approximately three times lower than an ideal monopole antenna. An ideal monopole built using SiP stack shown in Fig. 1(b) would have a far-field peak gain of 2.776 (4.41 dBi) based on simulation.

To meet the design rules of the commercial SiP fabrication process, particularly as it relates to the permissible metal density and spacing, small holes of 4 μm^2 are uniformly distributed over the metal layers (Fig.1(a)). The size of the holes, smaller than 1/10$^{\text{th}}$ of the antenna wavelength, will not affect the performance as the antenna can be considered a continuous surface.

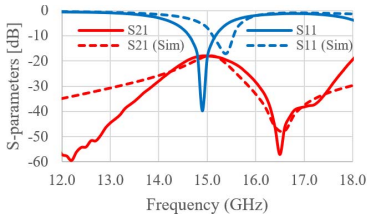

Fig. 2. Measured and simulated (Sim) S-parameters with antenna placed 0.3175 cm (0.125") apart.

The antenna is fed through a GSG probe for measurement purposes. In real applications, a photodetector replaces the GSG probe where the proximity of the PD to the antenna mitigates the need to have a transmission line and a matching network that tend to be lossy. In the measurements described next section, the body metal of the probe impacts the frequency response of the antenna and the radiation pattern due to the metal body being close to the antenna. To account for any variation in frequency due to the body of the probe or process variations of the SiP process, we maintain symmetry in the measurement setup described next. The proposed antenna operates in the radiative near field region. As such, conductors (e.g., GSG probes or other antennas) in the near field could lead to absorption of energy (signal leakage) and crosstalk. This will manifest itself as a change in the impedance of the antenna and a detuning of the operation frequency. Consequently, minimizing conductors in the near field region or implementing impedance adjustment circuits, as in [21], may be required for optimum antenna impedance matching.

III. Experimental Validation

The antennas are measured in two steps. First, the S-parameter measurements are taken using a vector network analyzer (VNA). Second, a PD is used as a transmitter with PRBS data transmission demonstrated. The calculated length defining the boundary between near-field and far-field is 6.6 mm [22]. Thus, S-parameters measurements characterize the coupling between antennas in the near-field. Antenna gain, as reported in fig. 1(c), is relevant for far-field distances beyond 6.6 mm.

S-parameters are measured by landing two identical GSG probes on two antennas. Identical probes were chosen for these measurements so that any variation in the frequency

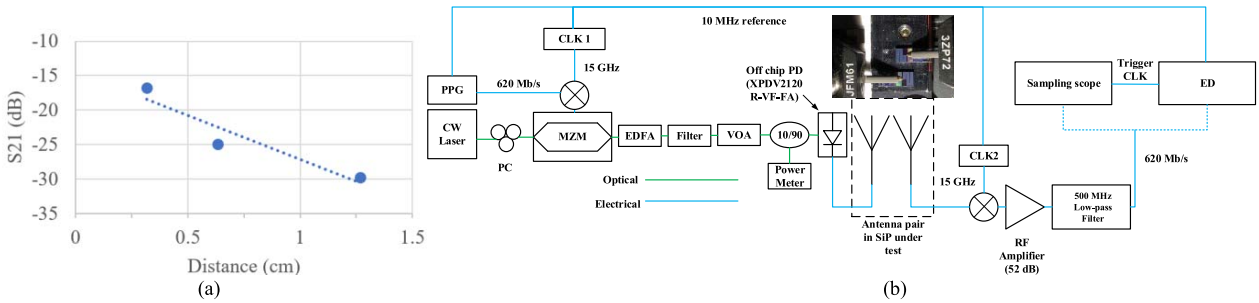

Fig. 3. (a) Measured peak S21 at 15 GHz at three different distances. (b) Measurements setup for inter-chip communication with an external photodetector as a transmitter directly driving the antenna. GSG probes were used to drive the antennas as shown above the antenna pair symbol.

response or the radiation pattern of the antenna pair due to the probes are matched. The antenna pair is placed at a distance of 0.3175 cm (0.125") from each other and aligned in the direction of maximum directivity in the y-axis as indicated by the gain pattern shown in Fig. 1(c). The antennas are arranged on the vacuum waveguide mount that uses air suction to hold them in place when landing the probes for measurements. Measured and simulated S11 (reflection coefficient) and S21 (forward transmission coefficient) curves are shown in Fig. 2. Both curves show general agreement with a frequency shift of 0.1 GHz for S21 and 0.3 GHz for S11 for the resonance frequency likely due to the GSG probes used for the measurement. S-parameter simulations consider only the second antenna placed in a vacuum without considering the presence of other probes and circuits in the near field of the antenna during measurements. Further, the HFSS simulation were limited by memory and processing power leading to inaccurate S21 prediction away from resonance. The measured 10 dB bandwidth of the antenna (S11 < -10 dB) is 600 MHz. The antenna shows a resonance at approximately 15 GHz and has an S21 peak of -16 dB. The transmission peak (S21) is measured for various distances as shown if Fig.3(a).

In the second measurement step, we use the setup shown in Fig. 3(b). to demonstrate inter-chip data transmission. For simplicity, a heterodyne transmission scheme is selected. In this setup, a 1550 nm continuous wave (CW) is modulated with a Mach–Zehnder modulator (MZM). The input to optical modulator is a 15 GHz RF carrier generated by a clock synthesizer (CLK 1, Anritsu 69377B) modulated with a 650 Mbps PRBS-7 data pattern generated by a programmable pattern generator (PPG, Keysight N4903B) using an RF mixer (Marki M90750) with 7.5 dB conversion loss. A relatively low bit rate is chosen as the antennas are narrow band. The carrier frequency is chosen to be 15 GHz as per the maximum S21 measured (Fig. 2). The output of the optical modulator (MZM) is amplified using an erbium-doped fiber amplifier (EDFA). The output of the EDFA is filtered with an optical filter centered around 1550 nm with an optical bandwidth (-3dB) of 0.69 nm. The output of the filter is connected to a variable optical attenuator (VOA) to control the optical power fed to an off-chip photodetector (Finisar XPDV2120R-VF-FA). The output of the VOA is fed to the PD through a 10/90 coupler. The 10 % output is monitored by an optical power meter. The photodetector has a reported typical responsivity of 0.65 A/W. The PD is internally matched to 50 Ω. This ensures proper matching between the PD and the antenna for maximum power transfer. On the receiver side, the output of the antenna is mixed with the same carrier frequency generated from CLK 2. The output of the mixer is amplified with an RF amplifier with 52 dB of gain and a bandwidth of 45 GHz. The signal is then filtered with a commercial low-pass filter with a cut-off frequency of 500 MHz. This is used to suppress frequency content at 30 GHz generated on the receiver side due to demodulation and any 15 GHz content due to clock feedthrough. Finally, the output is connected to an error detector (ED) and a sampling oscilloscope.

The measured bit-error-rate (BER) curves for 0.3175 cm (0.125") and 0.635 cm (0.25") are shown in Fig. 4. The antenna achieves a BER of 10^{-10} at a distance of 0.3175 cm. The BER worsens with the distance between the two antennas, to approximately 10^{-4} at 0.635 cm for the same input power. This relatively higher BER is because of the weak driving capability of the PD used directly as a transmitter without further pre-amplification to derive the antenna. In more conventional systems, a power amplifier is used to drive the antenna. Alternatively, high-power PDs could be used [8]–[10]. Another contributing factor is the smaller ground plane size than ideal that degrades the gain of the antenna. The captured and amplified eye diagram (Fig. 4) has an amplitude of 430 mV at 0.3175 cm and 270 mV at 0.635 cm, both for an input optical power of 10 dBm. At 1.27 cm (0.5"), the antenna is too far to allow for BER measurement. The ED fails to synchronize when the BER is above 10^{-3}. The BER is limited to 10^{-10} in the first case because the maximum power allowed at the PD is 10 dBm.

IV. Discussion

Important considerations of PD-antenna systems in SiP include area, gain, data-rate, and optical power needed for transmission. In terms of area and gain, at higher frequencies of operation such as the mm-wave frequencies of 60 GHz and higher, the size of the antenna can be reduced, and antenna arrays become feasible. Such arrays can be used to achieve better gain for more efficient inter-chip communication. It is also possible to bend the antenna as done in this design to reduce area, but with an adverse impact on gain. The data-rate is limited by the bandwidth of the antenna which can be increased by employing wider band structures, or higher frequency of operation. There are applications such as clock distribution [23] and wireless tagging [24] where low bandwidth is sufficient.

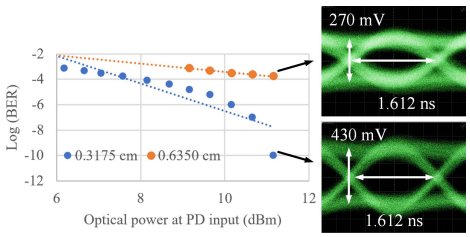

Fig. 4. Inter-chip antenna measured BER and eye diagrams curve for two different distances of antenna.

In terms of optical power, we estimate the minimum optical power required for RF transmission. We drive the transmitting antenna directly with an RF generator while connecting the receiving antenna to a spectrum analyzer. At 0.3175 cm, the RF generator needs to produce −27 dBm RF power for the signal to be distinguishable from the noise floor of the spectrum analyzer on the receiving end. The RF power, P_{RF}, is related to the RMS current, I_{RMS} through the input impedance of the antenna, Z, by $P_{RF} = (I_{RMS})^2 \times Z$. This gives an RMS current of 200 μA. The corresponding optical power, P_O, is then calculated using the responsivity of the PD ($P_O = I_{RMS}/R$). If a photodetector with a responsivity of 0.75 A/W were to be used, a minimum optical power of −5.75 dBm would be needed. If a PD with lower responsivity were to be used, then higher optical power would be needed (e.g. −3 dBm for $R = 0.4$ A/W). Note that for practical data transmission, higher power would be needed as indicated by the BER measurements (Fig. 4). Circuits such as a low noise amplifier on the receiver side or a power amplifier in the transmitter side can extend the communication distance between the two antennas. One can consider an equalizer to increase the limited bandwidth of the antenna.

V. Summary

In summary, this letter presents for the first time a 15 GHz monopole antenna in a commercial SiP. The antenna benefits from the high resistivity of the substrate of SiP to achieve improved performance. S-parameter measurements and inter-chip data transmission were both measured and demonstrated. Inter-chip communication is demonstrated while using a photodetector directly as a transmitter driving the antenna without RF amplification. Good matching (S11 < -10 dB) and peak gain (S21 $= 16$ dB) were achieved at 15 GHz. The simulated gain is 0.95 (−0.22 dBi). This validation points towards the possibility of developing monolithic photonic emitters in SiP consisting of an antenna and a photodetector.

As the silicon photonic process is relatively cheap, and the potential monolithic integration of PD and antenna eliminates the need for matching networks, the proposed concept could prove to be a cost-effective, area effective solution for inter-chip and RoF communication applications.

Acknowledgment

The authors would like to thank CMC Microsystems for the subsidized fabrication.

References

[1] M. Sanadgol Nezami *et al.*, "Integrated RF passive low-pass filters in silicon photonics," *IEEE Photon. Technol. Lett.*, vol. 30, no. 23, pp. 2052–2055, Dec. 1, 2018.

[2] L. Bogaert *et al.*, "Germanium photodetector with monolithically integrated narrowband matching network on a silicon photonics platform," in *Proc. Eur. Conf. Integr. Opt.*, 2019, pp. 1–3.

[3] M. M. P. Fard, G. Cowan, and O. Liboiron-Ladouceur, "Responsivity optimization of a high-speed germanium-on-silicon photodetector," *Opt. Express*, vol. 24, no. 24, Pp. 27738–27752, Nov. 2016.

[4] B. Radi, M. S. Nezami, M. Menard, F. Nabki, and O. Liboiron-Ladouceur, "A 12.5 Gb/s 1.93 pJ/bit optical receiver exploiting silicon photonic delay lines for clock phases generation replacement," *IEEE Trans. Circuits Syst. II, Exp. Briefs*, early access, Nov. 11, 2019, doi: 10.1109/TCSII.2019.2952591.

[5] M. S. Hai, M. Ménard, and O. Liboiron-Ladouceur, "Integrated optical deserialiser time sampling based SiGe photoreceiver," *Opt. Express*, vol. 23, no. 25, pp. 31736–31754, Dec. 2015.

[6] A. Babakhani, X. Guan, A. Komijani, A. Natarajan, and A. Hajimiri, "A 77-GHz phased-array transceiver with on-chip antennas in silicon: Receiver and antennas," *IEEE J. Solid-State Circuits*, vol. 41, no. 12, pp. 2795–2806, Dec. 2006.

[7] D. Jager, "Microwave photonics-from concepts to devices and applications," in *Microwave Photonics*. Boca Raton, FL, USA: CRC Press, Dec. 2017.

[8] A. Stöhr *et al.*, "Millimeter-wave photonic components for broadband wireless systems," *IEEE Trans. Microw. Theory Techn.*, vol. 58, no. 11, pp. 3071–3082, Nov. 2010.

[9] Q. Zhou, A. S. Cross, A. Beling, Y. Fu, Z. Lu, and J. C. Campbell, "High-power V-band InGaAs/InP photodiodes," *IEEE Photon. Technol. Lett.*, vol. 25, no. 10, pp. 907–909, May 15, 2013.

[10] Q. Li *et al.*, "High-power flip-chip bonded photodiode with 110 GHz bandwidth," *J. Lightw. Technol.*, vol. 34, no. 9, pp. 2139–2144, May 1, 2016.

[11] A. Stöhr, R. Heinzelmann, C. Kaczmarek, and D. Jäger, "Ultra-broadband Ka to W-band 1.55 [micro sign]m travelling-wave photomixer," *Electron. Lett.*, vol. 36, no. 11, pp. 970–971, 2000.

[12] N.-W. Chen, H.-J. Tsai, F.-M. Kuo, and J.-W. Shi, "High-speed *W*-band integrated photonic transmitter for Radio-Over-Fiber applications," *IEEE Trans. Microw. Theory Techn.*, vol. 59, no. 4, pp. 978–986, Apr. 2011.

[13] K. Li *et al.*, "High-power photodiode integrated with coplanar patch antenna for 60-GHz applications," *IEEE Photon. Technol. Lett.*, vol. 27, no. 6, pp. 650–653, Mar. 15, 2015.

[14] J. Moody, K. Sun, Q. Li, A. Beling, and S. M. Bowers, "A vivaldi antenna based W-band MUTC photodiode driven radiator," in *Proc. IEEE Int. Topical Meeting Microw. Photon. (MWP)*, Long Beach, CA, USA, Nov. 2016, pp. 217–220.

[15] T. Umezawa *et al.*, "Millimeter-wave integrated photoreceivers for high data rate photonic wireless communication," *IEEE J. Sel. Topics Quantum Electron.*, vol. 24, no. 2, pp. 1–9, Mar. 2018.

[16] M. Natrella *et al.*, "Modelling and measurement of the absolute level of power radiated by antenna integrated THz UTC photodiodes," *Opt. Express*, vol. 24, no. 11, p. 11793, May 2016.

[17] K. Sun, J. Moody, Q. Li, S. M. Bowers, and A. Beling, "High power integrated photonic W-Band emitter," *IEEE Trans. Microw. Theory Techn.*, vol. 66, no. 3, pp. 1668–1677, Mar. 2018.

[18] F. T. Ulaby, E. Michielssen, and U. Ravaioli, *Fundamentals of Applied Electromagnetics*, 6th ed. Upper Saddle River, NJ, USA: Prentice-Hall, 2001.

[19] I. Papapolymerou, R. Franklin Drayton, and L. P. B. Katehi, "Micromachined patch antennas," *IEEE Trans. Antennas Propag.*, vol. 46, no. 2, pp. 275–283, 2nd Quart., 1998.

[20] Nordic Semiconductor, Tiller, Norway. *λ/4 Printed Monopole Antenna for 2.45 GHz*. [Online]. Available: https://infocenter.nordicsemi.com/pdf/nwp_008.pdf?cp=12_18

[21] M. Gebhart, T. Baier, and M. Facchini, "Automated antenna impedance adjustment for near field communication (NFC)," in *Proc. 12th Int. Conf. Telecommun.*, Zagreb, Croatia, 2013, pp. 235–242.

[22] T. Lecklider, "The world of the near field," *Eval. Eng.*, vol. 10, pp. 100–106, Oct. 2005.

[23] B. A. Floyd, C.-M. Hung, and K. K. O, "Intra-chip wireless interconnect for clock distribution implemented with integrated antennas, receivers, and transmitters," *IEEE J. Solid-State Circuits*, vol. 37, no. 5, pp. 543–552, May 2002.

[24] Y. Toeda, T. Fujimaki, M. Hamada, and T. Kuroda, "Fully integrated OOK-powered pad-less deep sub-wavelength-sized 5-GHz RFID with on-chip antenna using adiabatic logic in 0.18μM CMOS," in *Proc. IEEE Symp. VLSI Circuits*, Jun. 2018, pp. 27–28.